Journal of Materials Chemistry C

PAPER

View Article Online
View Journal | View Issue

Cite this: J. Mater. Chem. C, 2019, 7, 11160

Tetraphenylpyrazine decorated 1,3-di(9*H*-carbazol-9-yl)benzene (mCP): a new AIE-active host with enhanced performance in organic light-emitting diodes†

Jiali Guo,‡[a] Lingxiang Pan,‡[a] Bo Song,[a] Jiabao Gu,[a] Jiajie Zeng,[a] Xiaotian Xu,[a] Haozhong Wu,[a] Zujin Zhao,[a] Zhiming Wang, *[a] Anjun Qin *[a] and Ben Zhong Tang *[ab]

Received 23rd May 2019,
Accepted 19th August 2019

DOI: 10.1039/c9tc02748c

rsc.li/materials-c

Aggregation-induced emission luminogens (AIEgens) have been widely used in organic light-emitting diodes (OLEDs), but few works have reported on utilizing AIEgens as hosts in doped OLEDs. In this work, a new AIEgen of **TPP-mCP** was designed and synthesized by integrating a typical AIE moiety of tetraphenylpyrazine (TPP) with a conventional host of 1,3-di(9*H*-carbazol-9-yl)benzene (**mCP**). **TPP-mCP** exhibits better thermal and conformational stability and carrier capacity, and higher emission efficiency in the film state than those of **mCP**. More importantly, the OLEDs fabricated with **TPP-mCP** as the host show much higher electroluminescent performance than those with **mCP**. Thus, this work not only generates a new AIE-active host of **TPP-mCP** with high device performance, but also provides a strategy to construct more effective hosts by decorating conventional ones with AIE units, which will potentially promote the development of OLEDs.

Introduction

Organic light-emitting diodes (OLEDs) have attracted unprecedented attention both in academic and industrial fields.[1,2] However, most of the conventional fluorophores suffer from the aggregation-caused quenching (ACQ) effect due to their strong intermolecular interactions, which limits their applications in OLEDs.[3,4] To overcome this difficulty, many chemical, physical and engineering methods have been applied but limited success was achieved. Different from the above methods, aggregation-induced emission (AIE) conceptually termed by our group in 2001 could actively use the molecular aggregation to promote the emission in the aggregate or solid state and has been proved to be an efficient strategy to tackle the ACQ effect.[5] The nature of AIE luminogens (AIEgens) is that they are non- or weakly emissive when molecularly dissolved but induced to emit intensely in the aggregate or solid state,[4] which greatly facilitates their applications in OLEDs.[6] Indeed, thanks to their intense emission in the solid state, plenty of AIEgens have been utilized in OLEDs as non-doped emitting layers with glorious electroluminescence (EL) performance.[6,7]

Moreover, the AIEgens could also be used as hosts to fabricate phosphorescent OLEDs (PhOLEDs). PhOLEDs are capable of utilizing both singlet and triplet excitons to achieve 100% internal quantum efficiency (IQE),[8] and have been successfully applied in solid-state lighting,[9] flat-panel display,[10] wearable devices[11] and so on.[12] Similar to the conventional fluorophores, most of the phosphorescent dyes also suffer from the ACQ effect. Thus, the host–guest strategy that disperses phosphorescent dyes into host materials is a way to reduce the quenching effect.[8,13] The hosts dominate the emitting layer (EML) and play a significant role in device performance of PhOLEDs. Thus, exploring efficient hosts that can satisfy the requirements of diverse phosphorescent dyes to improve their performance becomes highly desirable in PhOLEDs.[8d,e,13,14]

However, few works on this aspect have been performed.[15] Li *et al.* utilized the triphenylamine-based AIEgens as the hosts in PhOLEDs, and the maximum current, power efficiency and EQE of 57.4 cd A^{-1}, 52.0 lm W^{-1} and 18.2% were achieved, respectively. These values are higher than those of the devices with the conventional host of 4,4′-di(9*H*-carbazol-9-yl)-1,1′-biphenyl (CBP).[15b] Wang *et al.* synthesized a series of carbazole-based AIEgens and used them to construct red PhOLEDs with the

[a] State Key Laboratory of Luminescent Materials and Devices, Center for Aggregation-Induced Emission, South China University of Technology, Guangzhou 510640, China. E-mail: wangzhiming@scut.edu.cn, msqinaj@scut.edu.cn
[b] Department of Chemistry, Hong Kong Branch of Chinese National Engineering Research Center for Tissue Restoration and Reconstruction, Institute for Advanced Study, and Department of Chemical and Biological Engineering, The Hong Kong University of Science and Technology, Clear Water Bay, Kowloon, Hong Kong, China. E-mail: tangbenz@ust.hk

† Electronic supplementary information (ESI) available: ^{1}H and ^{13}C NMR spectra, HRMS spectra, device fabrication and characterization, other analysis data. CCDC 1886117 (**TPP-mCP**). For ESI and crystallographic data in CIF or other electronic format see DOI: 10.1039/c9tc02748c

‡ J. Guo and L. Pan contributed equally to this work.

highest EQE of 19.3%.[15c] Obviously, those AIEgens used as the hosts exhibit superior device performance over the conventional ones. These results encourage us to explore new AIE-active hosts to further improve the EL efficiency of OLEDs.

One of the effective strategies to generate AIE-active hosts is to modify conventional hosts by covalently binding with an AIE-active moiety to make the new molecules AIE-active,[4] which will facilitate more efficient charge transfer from the highly emissive hosts to the guest molecules. Herein, we tried to covalently integrate a typical AIE moiety of tetraphenylpyrazine (TPP) with a conventional host of 1,3-di(9*H*-carbazol-9-yl)benzene (**mCP**) to generate a bipolar AIEgen of **TPP-mCP**. As expected, **TPP-mCP** exhibits an obvious AIE feature, and its emission peaks in solution and solid states still locate in the valuable deep-blue region. Notably, the 5% weight loss temperature (T_d) and glass-transition temperature (T_g) of **TPP-mCP** are enhanced obviously compared to those of **mCP**, which would be beneficial for increasing the morphological stability in device fabrication and operation, further promoting device performance. Indeed, the devices with **TPP-mCP** as the host show better device performance than those with **mCP** as host with similar guest phosphors of PO-01 and Ir(piq)$_2$(acac). Thus, this work not only realizes PhOLEDs with improved performance but also provides a strategy to construct new effective hosts from conventional ones, which will promote the development of OLEDs.

Results and discussion

Synthesis

The synthetic routes to **TPP-mCP** are illustrated in Scheme 1. The intermediates of **2**, **3** and **TPP-Br** were synthesized according to the methods reported in the literature.[16] The Suzuki coupling of **3** and TPP-Br readily generated the target molecule of **TPP-mCP** in 76% yield. The detailed synthetic procedures are given in the Experimental section and ESI.† The structure of **TPP-mCP** was fully characterized by ^{1}H and ^{13}C NMR and high-resolution mass spectroscopy (HRMS) and satisfactory data were obtained (see ESI† for details). **TPP-mCP** is soluble in commonly used organic solvents, such as dichloromethane (DCM), tetrahydrofuran (THF), and chloroform, but insoluble in water.

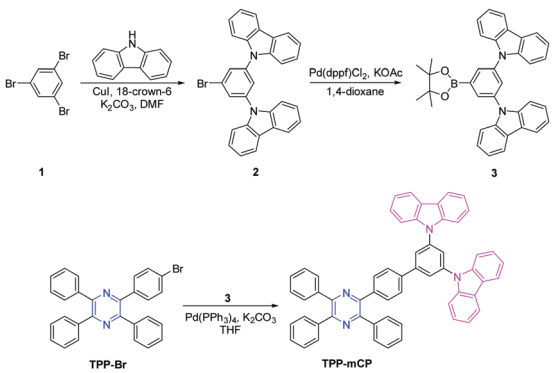

Scheme 1 Synthetic routes towards **TPP-mCP**.

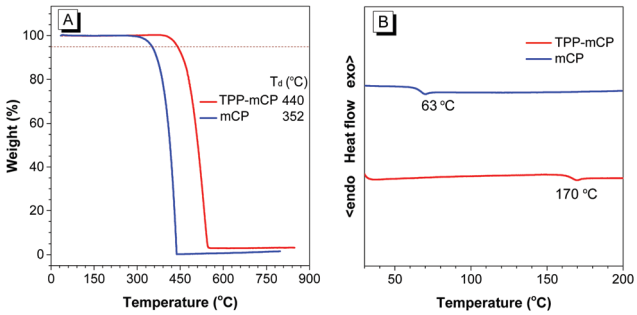

Fig. 1 (A) TGA and (B) DSC curves of **TPP-mCP** and **mCP** under nitrogen at a heating rate of 20 and 10 °C min^{-1}, respectively.

Thermal stability

Generally, good thermal and morphological stability of an emitter is essential to the process of vacuum deposition and the device operational stability. Moreover, the stability of a homogeneous dispersion system plays a crucial role in preventing the triplet–triplet annihilation (TTA) process.[8,17] Herein, the thermal stability of **TPP-mCP** and **mCP** was investigated by thermogravimetric analysis (TGA) and differential scanning calorimetry (DSC) with a heating rate of 20 and 10 °C min^{-1} under nitrogen, respectively. As can be seen from Fig. 1, **mCP** possesses a low T_g of 63 °C, which will generally decrease the performance of the devices because it will easily crystallize. In contrast, the T_g of **TPP-mCP** is as high as 170 °C. Furthermore, the T_d of **TPP-mCP** is 440 °C, which is 88 °C higher than that of **mCP**. Moreover, the excellent morphological stability of **TPP-mCP**-based systems was also confirmed by atomic force microscopy (AFM) measurement (Fig. S3–S5, ESI†). These results unambiguously indicate that **TPP-mCP** possesses superior thermal and morphological stability over **mCP**, which is favorable to the device fabrication, performance stability and EL efficiency.

Single crystal analysis

Considering that the molecular structures of hosts will have great influence on the device performance, we analyzed and compared the single crystal structures of **TPP-mCP** and **mCP**. The single crystal of **TPP-mCP** (CCDC 1886117†) was obtained during sublimation, and the crystal of **mCP** was cited from the reported literature.[18] The detailed data of X-ray diffraction analyses are shown in Fig. 2 and the ESI.† Similar to the TPP derivatives, four peripheral phenyl groups in **TPP-mCP** in its single crystal show a propeller shaped conformation with twisted angles in the range of 36–54° around the pyrazine center. The twist angles of the carbazole groups around the central phenyl ring are in the range of 40–61°. Regarding the single crystal of **mCP**, the twist angles of the coupled carbazole groups are in the range of 42–72°, which are larger than those of **TPP-mCP**.

When having a detailed insight into the molecular packing modes of **TPP-mCP** and **mCP**, we could find that the carbazole groups of the former enjoy parallel arrangements while those of **mCP** are randomly packed. In view of the twisted angles and packing models of **TPP-mCP** and **mCP**, the former should possess a higher carrier mobility. Moreover, multiple intermolecular C–H$\cdots\pi$

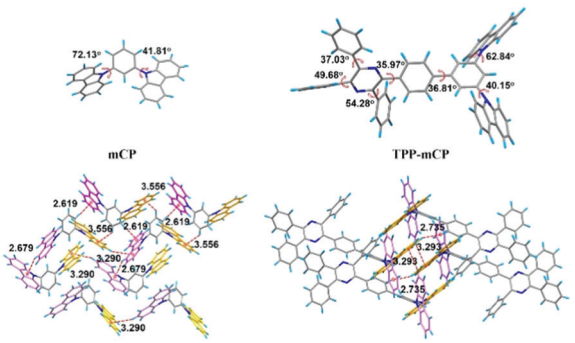

Fig. 2 Crystal structures, torsion angles and intermolecular C–H···π interactions of **mCP** and **TPP-mCP**.

interactions in **TPP-mCP** with distances of 2.74–3.29 Å between the molecules were observed (Fig. 2). Such interactions could help rigidify the molecular conformation, restrict the intramolecular rotation in the crystal lattice and thus reduce the non-radiative decay of excitons,[4,16a,19] resulting in enhanced emission in the aggregate state. In contrast, the distances of neighbor molecules in **mCP** are larger than those in **TPP-mCP**, suggesting that **mCP** adopts a looser packing model.

Photophysical properties

After confirming their structures and investigating their packing models in the crystalline states of **TPP-mCP** and **mCP**, we studied their photophysical properties. As demonstrated in Fig. 3 and Table 1, the absorption spectrum of **TPP-mCP** in THF solution has two main peaks with one located at 292 nm and the other at 339 nm. The former is a typical absorption of the carbazole group, and the latter could be attributed to the π–π* transition. Furthermore, **TPP-mCP** shows weak emission with a maximum peak at 425 nm and possesses a low Φ_F of 1.0% in THF solution because of its twisted structure and freely rotated aromatic rings, whereas, in the solid film state, the maximum emission peak of **TPP-mCP** remains almost unchanged but the Φ_F is enhanced to 12.0%, suggestive of an AIE feature. In sharp contrast, **mCP** is highly emissive in THF solution with a Φ_F value of 12.0%; however, its emission efficiency decreases to 9.0% upon aggregation, demonstrating an ACQ effect.

The AIE activity of **TPP-mCP** was further studied by measuring its photoluminescence (PL) behavior in THF/water mixtures with different water fraction (f_w). As depicted in Fig. 3, **TPP-mCP** shows faint emission in diluted THF solution, and its PL intensity increases slightly when the f_w is less than 60%. Once $f_w > 60\%$, the emission exhibits a rapid enhancement because of the formation of nanoaggregates, further confirming its AIE feature.

For the purpose of deep comparison of the photophysical properties of **TPP-mCP** and **mCP**, their fluorescence lifetime (τ) in solution and film states was evaluated by measuring their time-resolved fluorescence spectra (Fig. S6, ESI†). The results indicate that the lifetime of **TPP-mCP** is one order of magnitude smaller than that of **mCP**. The shorter lifetime and stronger emission intensity of **TPP-mCP** in the film state are conducive to more rapid and efficient Förster energy transfer from the **TPP-mCP** to the guest molecules in the doped OLEDs.[20]

Electronic structures

To have a detailed understanding on the **TPP-mCP** host at the molecular level, density functional theory (DFT) and time-dependent DFT (TD-DFT) calculations using the B3LYP/6-31G(d) method were carried out. As shown in Fig. 4, similar to its crystal structure, the optimized geometry of **TPP-mCP** in the gas phase also adopts an obvious twisted conformation with the angles of benzene rings about 36° and that of carbazole at about 55°, which could effectively obstruct the intermolecular π–π stacking interactions in the aggregate state. Furthermore, the electron cloud distributions of the highest occupied molecular orbital (HOMO) are primarily concentrated on one of the two carbazole moieties with some located on the π-bridged phenyl group, which provides a hole transport channel. Whereas, the lowest unoccupied molecular orbital (LUMO) is mainly located at the TPP core and the π-bridged phenyl group, which contributes to the electron-transport channel. According to the calculation, the band gap of **TPP-mCP** is 3.64 eV, which is promising for its use as a host in doped OLEDs.[8d]

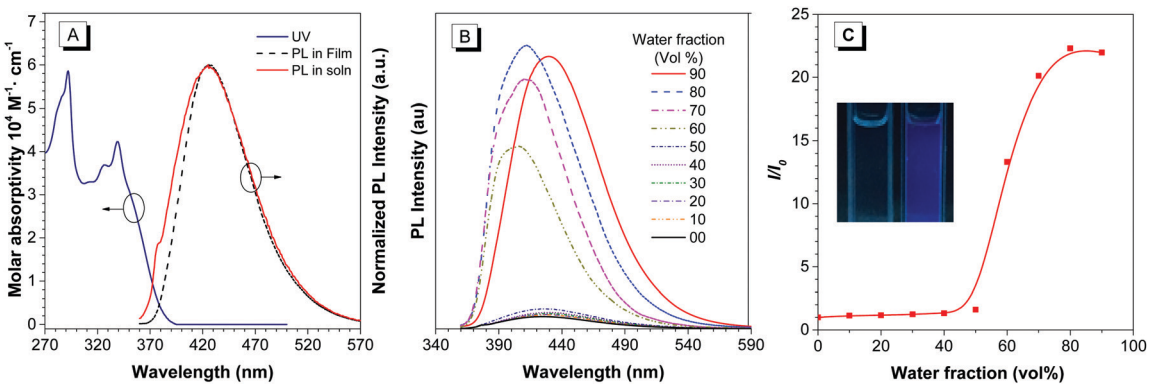

Fig. 3 (A) Absorption and photoluminescence (PL) spectra of **TPP-mCP** in THF solution (10 μM) and solid film. (B) PL spectra of **TPP-mCP** in THF/water mixtures with different water fractions; excitation wavelength: 339 nm; concentration: 10 μM. (C) Plot of relative intensity of **TPP-mCP** *versus* water fraction in THF/water mixtures; I_0 refers to the original emission intensity in THF.

Table 1 The photo-physical properties and thermal properties of **TPP-mCP** and **mCP**

Compound	λ_{abs}[a] [nm]	λ_{em}[b] [nm]		Φ_F[c] [%]		τ[d] [ns]		K_r[e] [10^7]		K_{nr}[f] [10^7]		T_g/T_d [°C]
		Soln	Film	Soln	Film	Soln	Film	Soln	Film	Soln	Film	
TPP-mCP	292, 339	425	426	1.0	12.0	0.83	0.83	1.20	14.48	119.28	106.02	170/440
mCP	325, 338	345, 360	383	12.0	9.0	6.92	6.07	1.73	1.48	12.72	15.00	63/352

[a] Absorption peaks, concentration: 10 μM. [b] Maximum emission wavelength, soln: THF solution, film: droplet film. [c] Absolute fluorescence quantum yield, determined by a calibrated integrating sphere. [d] Fluorescence lifetime, measured at room temperature in air. [e] $K_r = \Phi_F/\tau$. [f] $K_{nr} = (1 - \Phi_F)/\tau$.

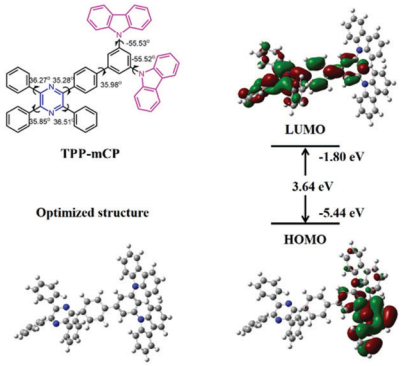

Fig. 4 HOMO/LUMO distributions and energy level of **TPP-mCP** in ground states.

Electrochemical behaviors

The energy level of **TPP-mCP** was also experimentally estimated using cyclic voltammetry (CV). As shown in Fig. 5, the cyclic voltammogram of **TPP-mCP** has reversible oxidation peaks, suggestive of its excellent electrochemical stability. The value of the HOMO is estimated to be −5.27 eV from the onset oxidation potential using the following equation of $E_{HOMO} = -(E_{onset} - E_{Fc/Fc^+} + 4.8)$ eV, with E_{onset} = 0.87 V and E_{Fc/Fc^+} = 0.40 V as tested, where Fc represents ferrocene. The LUMO energy level is thus calculated based on the onset of absorption of **TPP-mCP** to be −2.02 eV from the equation of $E_{HOMO} = E_{LUMO} + E_g$, where $E_g = 1240/\lambda_{onset}$. The HOMO and LUMO energy levels of **TPP-mCP** can match those of general transporting materials, which could help in selecting adjacent transporting materials and decreasing the driving voltage.

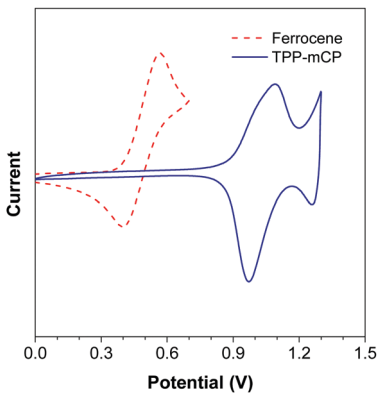

Fig. 5 Cyclic voltammograms of **TPP-mCP** and ferrocene, measured in dichloromethane containing 0.1 M tetra-*n*-butylammonium hexafluorophosphate.

Electroluminescence performance

Thanks to its excellent thermal and morphological stability, suitable energy levels, distinct AIE feature, short lifetime and intense emission in the aggregate state, **TPP-mCP** might be a kind of potential and efficient AIE-active host to promote device performance.

Considering the energy level and triplet energy matching up with **TPP-mCP** as well as the compared host of **mCP** (Fig. S7, ESI†), PO-01 and Ir(piq)$_2$(acac) were chosen as the yellow and red dopants to evaluate the performance of devices. As shown in Fig. S8 (ESI†), the absorption spectra of the phosphorescent dopants and the PL spectrum of the host **TPP-mCP** in solid film show excellent overlapping, indicating that the efficient energy transfer process from AIE-active host to dopants would be achieved in OLEDs. Subsequently, devices with configurations of ITO/HATCN (5 nm)/TAPC (25 nm)/TCTA (5 nm)/**TPP-mCP:** *x* wt% dopant (20 nm)/TmPyPB (55 nm)/LiF (1 nm)/Al were fabricated, where HATCN (1,4,5,8,9,11-hexaazatriphenylenehexacarbonitrile) is the hole injection layer (HIL), TAPC (1-bis[4-[*N*,*N*-di(4-tolyl)-amino]phenyl]cyclohexane) works as the hole-transporting layer (HTL), TCTA (tris(4-carbazoyl-9-ylphenyl)amine) serves as the electron-blocking layer (EBL), TmPyPB (1,3,5-tri(*m*-pyrid-3-yl-phenyl)benzene) acts as the electron-transporting layer (ETL) and the hole-blocking layer (HBL), and LiF is the electron injection layer (the chemical structures of them are shown in Fig. S9, ESI†).

As for the dopant of PO-01, three devices, O1, O2 and O3, with *x* = 6, 8 and 10, respectively, were fabricated. Whereas, for Ir(piq)$_2$(acac), four devices, R1, R2, R3 and R4, with *x* = 3, 6, 8 and 10, respectively, were generated. The energy levels of these materials and the device structures are given in Fig. 6. To highlight the performance of **TPP-mCP** host based devices, we also fabricated the devices with the conventional host of **mCP**, *i.e.* O5 and R5, under exactly the same experimental conditions, but where the composition of the EML of O5 is **mCP:** 8% wt PO-O1 and that of R5 is **mCP:** 3% wt Ir(piq)$_2$(acac).

Fig. 7 shows the results of **TPP-mCP**-hosted devices, and the detailed EL properties of them are summarized in Table S1, and Fig. S10 and S11 (ESI†). As can be seen, all the devices exhibit a low turn-on voltage (V_{on}) of about 3.0 V owing to the small energy barrier between the transporting and emitting layers, indicative of the efficient charge injection. The EL spectra of these doped devices (Fig. 7A) kept constant at varied luminance,

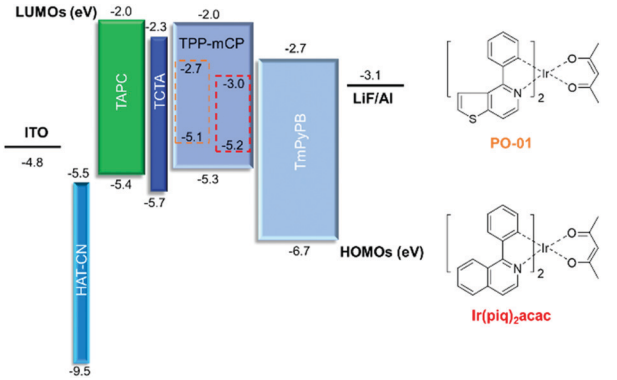

Fig. 6 Schematic energy level diagrams of the devices investigated and the chemical structures of phosphorescent guests used in this work. The HOMO and LUMO of phosphorescent dopants are displayed by dashed lines.

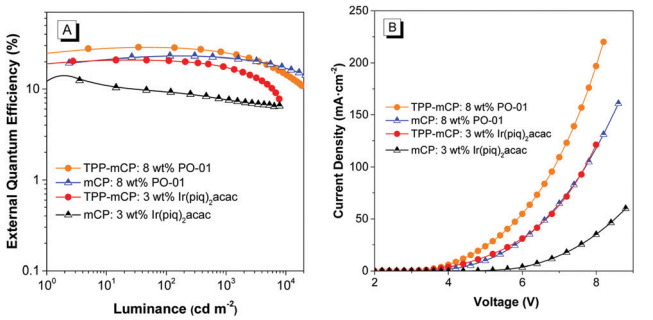

Fig. 8 (A) Plots of luminance *versus* external quantum efficiency; (B) changes in current density with the applied voltages of **TPP-mCP**-hosted devices and **mCP**-hosted devices. Device configuration: ITO/HATCN (5 nm)/TAPC (25 nm)/TCTA (5 nm)/EML (20 nm)/TmPyPB (55 nm)/LiF (1 nm)/Al.

suggestive of their good colour stabilities. Among the fabricated **TPP-mCP**-hosted devices, O2 (with 8 wt% PO-01) and R1 (with 3 wt% Ir(piq)$_2$(acac)) performed the best.

Importantly, when comparing the performance of **TPP-mCP**-hosted devices with that of **mCP**-hosted ones (Fig. 8 and Table 2), it is obvious that the **TPP-mCP**-hosted devices demonstrate much better performance than those hosted by **mCP**. Notably, the device O2 exhibits an outstanding maximum power efficiency ($\eta_{p,max}$) of 104.21 lm W^{-1}, current efficiency ($\eta_{c,max}$) of 89.54 cd A^{-1} and external quantum efficiency ($\eta_{ext,max}$) of 28.72%, which are apparently better than those of device O5 hosted by **mCP** ($\eta_{p,max}$: 66.49 lm W^{-1}; $\eta_{c,max}$: 70.62 cd A^{-1}; $\eta_{ext,max}$: 23.07%) with the same CIE coordinates. What's more, the **TPP-mCP**-hosted devices still remain higher in EL efficiency even under a high luminance of 5000 cd m^{-2}, which is of practical value. Similarly, device R1 also shows better efficiencies than R5. For example, $\eta_{ext,max}$ of 20.87% of R1 is much higher than that of device R5 (12.44%) at almost the same CIE coordinates. These excellent performances indicate that the AIE-active **TPP-mCP** host is a promising candidate in the fabrication of doped OLEDs.

In addition, the hole-only (HODs) and electron-only devices (EODs) were fabricated to confirm the bipolar behavior of

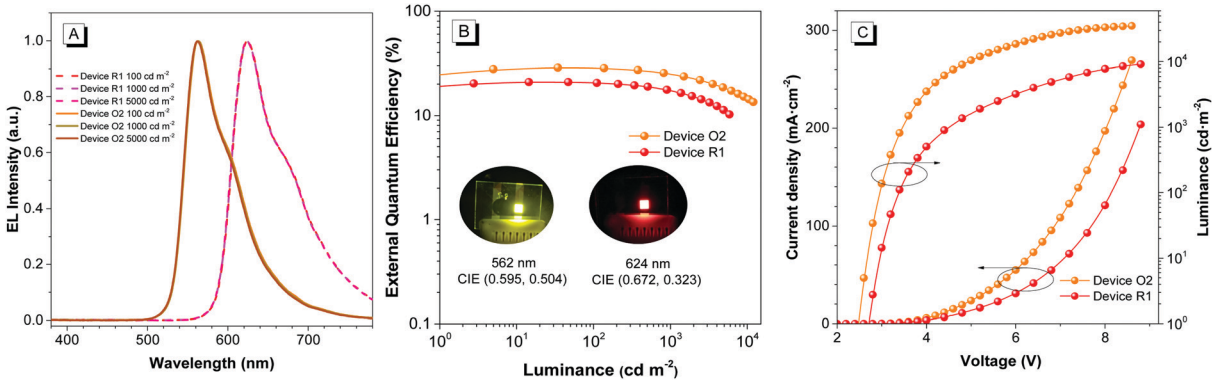

Fig. 7 (A) Plots of electroluminescence (EL) spectra at various voltages; (B) luminance *versus* external quantum efficiency; (C) changes in current density and luminance with the applied voltages of **TPP-mCP**-hosted devices O2 and R1. Device configuration: ITO/HATCN (5 nm)/TAPC (25 nm)/TCTA (5 nm)/**TPP-mCP**:dopant (20 nm)/TmPyPB (55 nm)/LiF (1 nm)/Al. Dopant = 8 wt% PO-01 (O2), 3 wt% Ir(piq)$_2$acac (R1).

Table 2 Comparison of EL performance of **TPP-mCP**-hosted and **mCP**-hosted devices

Device[a]	Host	V_{on}[b] (V)	$\eta_{c,max}$[c] (cd A^{-1})	$\eta_{p,max}$[d] (lm W^{-1})	η_{ext}[e] (%)	λ_{max}[f] (nm)	CIE[f] (x, y)
O2	**TPP-mCP**	2.6	89.54	104.21	28.72	562	(0.495, 0.504)
O5	**mCP**	2.6	70.62	66.49	23.07	562	(0.492, 0.504)
R1	**TPP-mCP**	2.8	15.68	16.96	20.87	624	(0.672, 0.323)
R5	**mCP**	4.4	9.05	6.47	12.44	622	(0.668, 0.328)

[a] O2 and R1 represent the **TPP-mCP**-hosted devices, O5 and R5 represent the **mCP**-hosted devices. [b] The turn-on voltage at 1 cd m^{-2}. [c] Maximum current efficiency. [d] Maximum power efficiency. [e] Maximum external quantum efficiency. [f] EL maximum wavelength and Commission Internationale de l'Eclairage coordinates at 10 mA cm^{-2}.

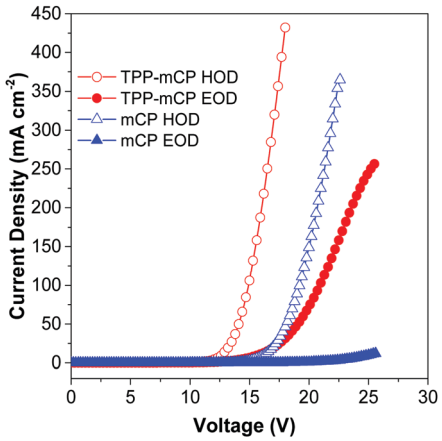

Fig. 9 Current density *versus* voltage characteristics of HODs and EODs of **TPP-mCP** and **mCP** hosts.

TPP-mCP and compare the carrier transporting abilities of **TPP-mCP** and **mCP** (the device structures are given in the ESI†). As shown in Fig. 9, **mCP** possesses a high hole current density and extremely low electron current density, suggesting that it has obviously unbalanced hole and electron transporting properties. This unbalanced hole and electron transporting ability of **mCP** agrees well with the literature.[21] Notably, the **TPP-mCP** host not only exhibits significantly higher electron current density, but also shows better balanced charge transporting properties, indicative of a more bipolar feature than that of **mCP**. This property is beneficial for balanced carrier mobility in the emitting layer of the **TPP-mCP**-based devices. These results are also consistent with our discussion about the crystal packing models of **TPP-mCP** and **mCP**, in which the carbazole groups of the former enjoy parallel arrangements while those of the latter are random, which might be one of the factors accounting for the superior EL performance of **TPP-mCP**-hosted devices over **mCP**-hosted ones. Furthermore, the current density in **TPP-mCP**-hosted devices is obvious higher than that in **mCP**-hosted ones, as shown in Fig. 8B, further comfirming the above conclusion.

For those host–guest systems, the Förster energy transfer should play a pivotal role because most PhOLEDs are doped at a low concentration, leaving relatively long distances between the host and the guest molecules.[22] The efficiency of the Förster energy transfer process is usually measured by the rate (k_{ET}), the efficiency (Φ_{ET}) of Förster energy transfer and the Förster radius (R_0). The k_{ET} from a guest to a guest can be calculated using the following equation:[23]

$$K_{ET} = \frac{1}{\tau_D}\left(\frac{R_0}{R_{DA}}\right)^6 \quad (1)$$

where τ_D is the intrinsic radiative decay lifetime of the hosts in the absence of guests, R_0 is the Förster radius and R_{DA} is the host-to-guest distance.[24]

The calculated values of R_0, k_{ET}, and Φ_{ET} of those host–guest systems are listed in Table 3 (the detailed calculations of R_0 and Φ_{ET} are shown in the ESI†). According to eqn (1), the singlet fluorescence lifetime (τ_D) in solid film plays a critical role in determining the rate of Förster energy transfer of those host–guest systems. Thanks to the fact that the τ_D (0.83 ns) of **TPP-mCP** is one order of magnitude smaller than that (6.07 ns) of **mCP** (Table 1), the rate of Förster energy transfer (k_{ET}) from host molecules to guest molecules of **TPP-mCP**-based systems is one order of magnitude higher than that of **mCP** based ones. And the R_0 in **TPP-mCP** host–guest systems is slightly higher than that in **mCP**-hosted ones, which also contributes to the higher k_{ET}. In addition, the Förster energy transfer efficiency of **TPP-mCP**-hosted systems is also higher than that of **mCP**-hosted ones, with the Φ_{ET} values of about 95% and 80%, respectively. Thus, it is clear that more efficient Förster energy transfer from host to guest molecules can be achieved in the **TPP-mCP**-hosted systems than that in **mCP**-hosted ones, which could be another factor that contributes to the superior EL performance of **TPP-mCP**-hosted devices over **mCP**-hosted ones. This result also confirms that AIE-active **TPP-mCP** can be used as an efficient host in doped OLEDs.

Table 3 Förster energy transfer parameters of the host–guest systems

Host	Guest	R_0[a] (nm)	K_{ET}[b] (s^{-1})	Φ_{ET}[c] (%)
TPP-mCP	PO-01	2.64	3.30×10^{10}	96.48
	$Ir(piq)_2acac$	2.80	6.72×10^{9}	84.80
mCP	PO-01	2.55	2.40×10^{9}	94.30
	$Ir(piq)_2acac$	2.63	5.61×10^{8}	79.52

[a] Förster radius. [b] Rate of Förster energy transfer. [c] Efficiency of Förster energy transfer.

Conclusions

In summary, a new bipolar AIE-active host of **TPP-mCP** was designed and synthesized by integrating a typical AIE moiety of TPP with a conventional host of **mCP**. The characterization results show that the introduction of the TPP moiety endows **TPP-mCP** with higher thermal and morphological stabilities and better carrier capacity than that of the pristine **mCP**. Moreover, the higher absolute fluorescence quantum yield in solid film state and shorter radiative decay lifetime of **TPP-mCP** than those of **mCP** facilitate more rapid and efficient energy transfer from the host to guest molecules in the **TPP-mCP**-doped OLEDs than in **mCP**-doped ones. As a result, the performance of **TPP-mCP**-hosted devices is much better than that of **mCP**-hosted ones. Furthermore, the yellow OLED based on **TPP-mCP** (host) and PO-01 (dopant) exhibits the most remarkable device efficiency with $\eta_{c,max}$, $\eta_{p,max}$ and $\eta_{ext,max}$ of 89.5 cd A^{-1}, 104.2 lm W^{-1} and 28.7%, respectively. The excellent performance of **TPP-mCP**-hosted devices suggests that we have developed a new efficient host design strategy, which is introducing a typical AIE moiety to a conventional host molecule. This strategy will enlighten researchers on the design and synthesis of more efficient AIE-active hosts from conventional ACQ ones.

Conflicts of interest

There are no conflicts to declare.

Acknowledgements

This work is financially supported by the National Natural Science Foundation of China (21788102 and 51673118), Natural Science Fund of Guangdong Province (2019B030301003 and 2016A030312002), the Innovation and Technology Commission of Hong Kong (ITC-CNERC14SC01), Science & Technology Program of Guangzhou (201804020027, 201804010218 and 201704030069), and the Fundamental Research Funds for the Central Universities (2017JQ013). J. Guo thanks Mr Xinyi Cai for the instructive discussion.

Notes and references

1 (*a*) N. Sun, Q. Wang, Y. Zhao, Y. Chen, D. Yang, F. Zhao, J. Shan and D. Ma, *Adv. Mater.*, 2014, **26**, 1617; (*b*) L. Chen, G. Lin, H. Peng, S. Ding, W. Luo, R. Hu, S. Chen, F. Huang, A. Qin, Z. Zhao and B. Z. Tang, *Adv. Funct. Mater.*, 2017, **1**, 176; (*c*) J. Guo, Z. Zhao and B. Z. Tang, *Adv. Opt. Mater.*, 2018, **6**, 1800264; (*d*) X. Cai and S. J. Su, *Adv. Funct. Mater.*, 2018, **28**, 1802558.

2 (*a*) H. J. In, K. H. Oh, O. K. Kwon, C. H. Hyun and S. C. Kim, *IEEE Trans. Consum. Electron.*, 2010, **56**, 1191; (*b*) J. H. Jou, C. Y. Hsieh, J. R. Tseng, S. H. Peng, Y. C. Jou, J. H. Hong, S. M. Shen, M. C. Tang, P. C. Chen and C. H. Lin, *Adv. Funct. Mater.*, 2013, **23**, 2750.

3 (*a*) S. W. Thomas, G. D. Joly and T. M. Swager, *Chem. Rev.*, 2007, **107**, 1339; (*b*) J. Yang, L. Li, Y. Yu, Z. Ren, Q. Peng, S. Ye, Q. Li and Z. Li, *Mater. Chem. Front.*, 2017, **1**, 91.

4 (*a*) J. Mei, N. L. Leung, R. T. Kwok, J. W. Lam and B. Z. Tang, *Chem. Rev.*, 2015, **115**, 11718; (*b*) D. Ding, K. Li, B. Liu and B. Z. Tang, *Acc. Chem. Res.*, 2013, **46**, 2441; (*c*) Y. Hong, J. W. Y. Lam and B. Z. Tang, *Chem. Soc. Rev.*, 2011, **40**, 5361.

5 J. Luo, Z. Xie, J. W. Lam, L. Cheng, H. Chen, C. Qiu, H. S. Kwok, X. Zhan, Y. Liu, D. Zhu and B. Z. Tang, *Chem. Commun.*, 2001, 1740.

6 (*a*) Z. Zhao, J. W. Lam and B. Z. Tang, *J. Mater. Chem. C*, 2012, **22**, 23726; (*b*) Q. Zhao and J. Z. Sun, *J. Mater. Chem. C*, 2016, **4**, 10588.

7 (*a*) J. Huang, H. Nie, J. Zeng, Z. Zhuang, S. Gan, Y. Cai, J. Guo, S. J. Su, Z. Zhao and B. Z. Tang, *Angew. Chem., Int. Ed.*, 2017, **56**, 12971; (*b*) G. Lin, H. Peng, L. Chen, H. Nie, W. Luo, Y. Li, S. Chen, R. Hu, A. Qin, Z. Zhao and B. Z. Tang, *ACS Appl. Mater. Interfaces*, 2016, **8**, 16799; (*c*) T. Liu, L. Zhu, C. Zhong, G. Xie, S. Gong, J. Fang, D. Ma and C. Yang, *Adv. Funct. Mater.*, 2017, **27**, 1606384; (*d*) Z. Peng, K. Huang, Y. Tao, X. Li, L. Zhang, P. Lu and Y. Wang, *Mater. Chem. Front.*, 2017, **1**, 1858; (*e*) L. Yao, S. Zhang, R. Wang, W. Li, F. Shen, B. Yang and Y. Ma, *Angew. Chem., Int. Ed.*, 2014, **53**, 2119.

8 (*a*) Y. G. Ma, H. Y. Zhang, J. C. Shen and C. M. Che, *Synth. Met.*, 1998, **94**, 245; (*b*) M. A. Baldo, D. F. O'Brien, Y. You, A. Shoustikov, S. Sibley, M. E. Thompson and S. R. Forrest, *Nature*, 1998, **395**, 151; (*c*) Y. Tao, C. Yang and J. Qin, *Chem. Soc. Rev.*, 2011, **40**, 2943; (*d*) Y. Tao, Q. Wang, C. Yang, Q. Wang, Z. Zhang, T. Zou, J. Qin and D. Ma, *Angew. Chem., Int. Ed.*, 2008, **47**, 8104–8107; (*e*) H. Liu, G. Cheng, D. Hu, F. Shen, Y. Lv, G. Sun, B. Yang, P. Lu and Y. Ma, *Adv. Funct. Mater.*, 2012, **22**, 2830.

9 C. Branas, F. J. Azcondo and J. M. Alonso, *IEEE Ind. Electron. Mag.*, 2013, **7**, 6.

10 (*a*) K. T. Kamtekar, A. P. Monkman and M. R. Bryce, *Adv. Mater.*, 2010, **22**, 572; (*b*) M. Zhu and C. Yang, *Chem. Soc. Rev.*, 2013, **42**, 4963.

11 J. K. Borchardt, *Mater. Today*, 2004, **7**, 42.

12 (*a*) H. Fu, Y. M. Cheng, P. T. Chou and Y. Chi, *Mater. Today*, 2011, **14**, 472; (*b*) V. C. Bender, N. D. Barth, F. B. Mendes, R. A. Pinto, J. M. Alonso and T. B. Marchesan, *IEEE J. Emerging Sel. Top. Power Electron.*, 2018, **6**, 1252.

13 (*a*) L. Xiao, Z. Chen, B. Qu, J. Luo, S. Kong, Q. Gong and J. Kido, *Adv. Mater.*, 2011, **23**, 926; (*b*) H. Sasabe and J. Kido, *J. Mater. Chem. C*, 2013, **1**, 1699–1707.

14 (*a*) W. Li, J. Li, D. Liu and Q. Jin, *ACS Appl. Mater. Interfaces*, 2016, **8**, 22382; (*b*) G. Nagatsu, T. Sakanoue, S. Tane, F. Yonekawa and T. Takenobu, *Mater. Chem. Front.*, 2018, **2**, 952; (*c*) Y. Li, D. Zhang, Y. Zhang, M. Cai and L. Duan, *Sci. China: Chem.*, 2016, **59**, 684; (*d*) Y. Hu, Y. Yuan, Y. L. Shi, J. D. Lin, Z. Q. Jiang and L. S. Liao, *J. Mater. Chem. C*, 2018, **6**, 1407; (*e*) C. Adachi, R. C. Kwong, P. Djurovich, V. Adamovich, M. A. Baldo, M. E. Thompson and S. R. Forrest, *Appl. Phys. Lett.*, 2001, **79**, 2082.

15 (*a*) J. Huang, X. Yang, X. Li, P. Chen, R. Tang, F. Li, P. Lu, Y. Ma, L. Wang, J. Qin, Q. Li and Z. Li, *Chem. Commun.*, 2012, **48**, 9586; (*b*) X. Zhan, Z. Wu, Y. Lin, Y. Xie, Q. Peng, Q. Li, D. Ma and Z. Li, *Chem. Sci.*, 2016, **7**, 4355; (*c*) C. Wu, Z. Wu, B. Wang, X. Li, N. Zhao, J. Hu, D. Ma and Q. Wang, *ACS Appl. Mater. Interfaces*, 2017, **9**, 32946.

16 (*a*) M. Chen, H. Nie, B. Song, L. Li, J. Z. Sun, A. Qin and B. Z. Tang, *J. Mater. Chem. C*, 2016, **4**, 2901; (*b*) L. Pan, W. Luo, M. Chen, J. Liu, L. Xu, R. Hu, Z. Zhao, A. Qin and B. Z. Tang, *Chin. J. Org. Chem.*, 2016, **36**, 1316; (*c*) L. Pan, Y. Cai, H. Wu, F. Zhou, A. Qin, Z. Wang and B. Z. Tang, *Mater. Chem. Front.*, 2018, **2**, 1310; (*d*) L. Pan, H. Wu, J. Liu, K. Xue, W. Luo, P. Chen, Z. Wang, A. Qin and B. Z. Tang, *Adv. Opt. Mater.*, 2019, 1801673.

17 M. Kim and J. Y. Lee, *Adv. Funct. Mater.*, 2014, **24**, 4164.

18 (*a*) Y. Sun, X. Zhu, Z. Chen, Y. Zhang and Y. Cao, *J. Org. Chem.*, 2006, **71**, 6281; (*b*) V. Adamovich, J. Brooks, A. Tamayo, A. Alexander, P. Djurovich, B. D'Andrade, C. Adachi, S. Forrest and M. Thompson, *New J. Chem.*, 2002, **26**, 1171–1178.

19 M. Chen, L. Li, H. Nie, J. Tong, L. Yan, B. Xu, J. Sun, W. Tian, Z. Zhao, A. Qin and B. Z. Tang, *Chem. Sci.*, 2015, **6**, 1932.

20 M. Kim and J. Y. Lee, *Adv. Funct. Mater.*, 2014, **24**, 4164.

21 Y. Zhao, C. Wu, P. Qiu, X. Li, Q. Wang, J. Chen and D. Ma, *ACS Appl. Mater. Interfaces*, 2016, **8**, 2635.

22 (*a*) Y. Kawamura, S. Yanagida and S. R. Forrest, *J. Appl. Phys.*, 2002, **92**, 87; (*b*) C. Han, F. Zhao, Z. Zhang, L. Zhu, H. Xu, J. Li, D. Ma and P. Yan, *Chem. Mater.*, 2013, **25**, 4966; (*c*) W. S. Jeon, T. J. Park, S. Y. Kim, R. Pode, J. Jang and J. H. Kwon, *Org. Electron.*, 2009, **10**, 240.

23 T. Förster, *Discuss. Faraday Soc.*, 1959, **27**, 7.

24 T. Förster, *Ann. Phys.*, 1948, **2**, 55.

